ARTICLES
PUBLISHED ONLINE: 2 NOVEMBER 2015 | DOI: 10.1038/NPHYS3527
nature physics

Characterization of collective ground states in single-layer $NbSe_2$

Miguel M. Ugeda[1,2,3]*, Aaron J. Bradley[1], Yi Zhang[4,5,6], Seita Onishi[1], Yi Chen[1], Wei Ruan[1,7], Claudia Ojeda-Aristizabal[1,8,9], Hyejin Ryu[4], Mark T. Edmonds[1,10], Hsin-Zon Tsai[1], Alexander Riss[1,11], Sung-Kwan Mo[4], Dunghai Lee[1], Alex Zettl[1,8,12], Zahid Hussain[4], Zhi-Xun Shen[5,13] and Michael F. Crommie[1,8,12]*

Layered transition metal dichalcogenides are ideal systems for exploring the effects of dimensionality on correlated electronic phases such as charge density wave (CDW) order and superconductivity. In bulk $NbSe_2$ a CDW sets in at $T_{CDW} = 33$ K and superconductivity sets in at $T_c = 7.2$ K. Below T_c these electronic states coexist but their microscopic formation mechanisms remain controversial. Here we present an electronic characterization study of a single two-dimensional (2D) layer of $NbSe_2$ by means of low-temperature scanning tunnelling microscopy/spectroscopy (STM/STS), angle-resolved photoemission spectroscopy (ARPES), and electrical transport measurements. We demonstrate that 3 × 3 CDW order in $NbSe_2$ remains intact in two dimensions. Superconductivity also still remains in the 2D limit, but its onset temperature is depressed to 1.9 K. Our STS measurements at 5 K reveal a CDW gap of $\Delta = 4$ meV at the Fermi energy, which is accessible by means of STS owing to the removal of bands crossing the Fermi level for a single layer. Our observations are consistent with the simplified (compared to bulk) electronic structure of single-layer $NbSe_2$, thus providing insight into CDW formation and superconductivity in this model strongly correlated system.

Many-body electronic ground states can be sensitive to the spatial dimensions of a material[1–5]. In transition metal dichalcogenide materials, for example, significant differences are expected in charge density wave and superconducting (SC) phases as dimensionality is reduced from a bulk three-dimensional (3D) material to a single-layer 2D material[6–9]. $NbSe_2$ is a model system in this regard, as it has been predicted to preserve its charge density wave (CDW) order in the single-layer limit, although with a significantly shortened CDW wavevector ($\mathbf{q}_{CDW}$; ref. 6). A metal to semi-metal transition has also been predicted for $NbSe_2$ when it is reduced to the 2D limit[6,7,10]. Previous work has shown that the superconducting transition temperature for $NbSe_2$ decreases from its bulk value of $T_C = 7.2$ K as the thickness is reduced[11–13], but no experimental studies have yet been performed that explore the interplay between $NbSe_2$ superconductivity and CDW formation in the extreme 2D limit.

CDW behaviour in the 3D limit of $NbSe_2$, on the other hand, has been well studied, although the origin of the bulk CDW transition at $T_{CDW} = 33$ K remains controversial. Recent experiments suggest that electron–phonon coupling plays a dominant role in triggering the CDW phase[14–20], thus casting doubt on mechanisms involving Fermi-surface nesting[21–24] and saddle-point singularities[25,26]. Critical experimental parameters associated with the CDW, such as the magnitude and location of the energy gap, also remain unclear. Previous STS measurements on bulk $NbSe_2$ in the CDW phase have revealed an unexpectedly large gap-like structure having width $2\Delta \sim 70$ meV (refs 27,28), although a recent analysis of STS data suggests that the CDW energy gap is only $2\Delta \approx 24$ meV (ref. 18). In contrast, low-temperature angle-resolved photoemission spectroscopy (ARPES) measurements performed on bulk $NbSe_2$ show an anisotropic CDW energy gap at E_F with a width of only a few meV (ref. 17). In general, it is expected that a weak-coupling CDW derived from Fermi-surface nesting should open a small gap on the Fermi surface, whereas a strong-coupling CDW caused by electron–phonon coupling should open a larger gap away from the Fermi surface.

Here we report measurement of the electronic structure of single-layer $NbSe_2$ using a combination of scanning tunnelling microscopy/spectroscopy (STM/STS), ARPES and electronic transport techniques. This allows us to directly probe the electronic ground state of $NbSe_2$ in the 2D limit, enabling interrogation of the effects of dimensionality and interlayer coupling in this layered material. We observe a reduction in the number of Fermi-level-crossing bands from three (for bulk) to one in the single-layer limit. Despite this change in electronic structure, CDW order in single-layer $NbSe_2$ remains unchanged with respect to the bulk case. The simplified band structure of single-layer $NbSe_2$, however, allows unprecedented access to the $NbSe_2$ CDW energy gap by

[1]Department of Physics, University of California at Berkeley, Berkeley, California 94720, USA. [2]CIC nanoGUNE, 20018 Donostia-San Sebastian, Spain. [3]Ikerbasque, Basque Foundation for Science, 48011 Bilbao, Spain. [4]Advanced Light Source, Lawrence Berkeley National Laboratory, Berkeley, California 94720, USA. [5]Stanford Institute for Materials and Energy Sciences, SLAC National Accelerator Laboratory, Menlo Park, California 94025, USA. [6]National Laboratory of Solid State Microstructures, School of Physics, Collaborative Innovation Center of Advanced Microstructures, Nanjing University, Nanjing 210093, China. [7]State Key Laboratory of Low Dimensional Quantum Physics, Department of Physics, Tsinghua University, Beijing 100084, China. [8]Materials Sciences Division, Lawrence Berkeley National Laboratory, Berkeley, California 94720, USA. [9]Department of Physics & Astronomy, California State University Long Beach, Long Beach, California 90840, USA. [10]School of Physics and Astronomy, Monash University, Clayton, Victoria 3800, Australia. [11]Institute of Applied Physics, Vienna University of Technology, 1040 Wien, Austria. [12]Kavli Energy NanoSciences Institute at the University of California Berkeley and the Lawrence Berkeley National Laboratory, Berkeley, California 94720, USA. [13]Geballe Laboratory for Advanced Materials, Departments of Physics and Applied Physics, Stanford University, Stanford, California 94305, USA.
*e-mail: mmugeda@berkeley.edu; crommie@berkeley.edu

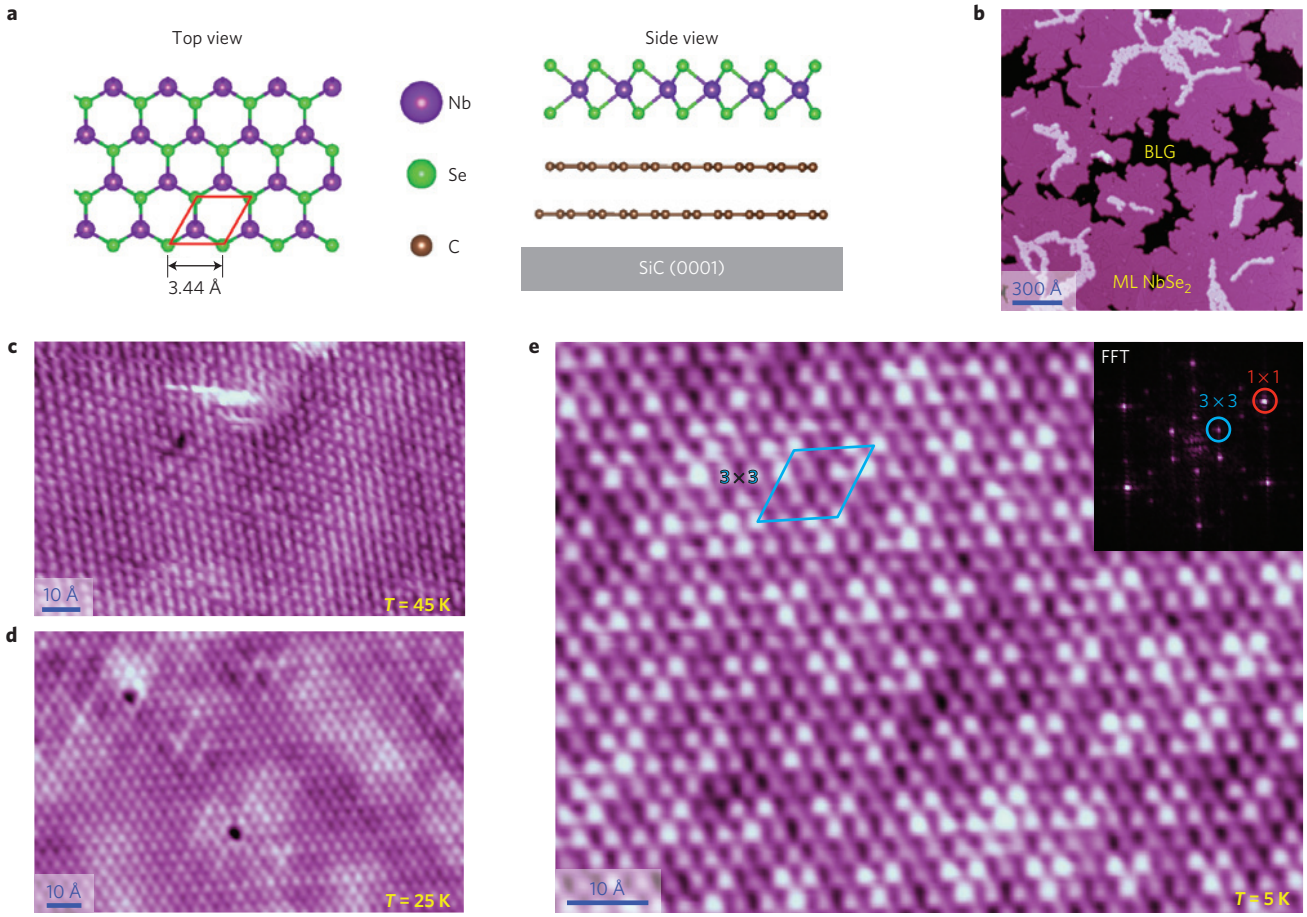

Figure 1 | Structure of single-layer $NbSe_2$ on bilayer graphene. a, Top and side view sketches of single-layer $NbSe_2$, including the substrate. **b**, Large-scale STM image of 0.9 ML of $NbSe_2$/BLG ($V_s = -100$ mV, $I_t = 3$ nA, $T = 5$ K). **c**–**e**, Atomically resolved STM images of single-layer $NbSe_2$ for different temperatures: $T = 45$ K ($V_s = +95$ mV, $I_t = 53$ pA) (**c**), $T = 25$ K ($V_s = -120$ mV, $I_t = 70$ pA) (**d**) and $T = 5$ K ($V_s = -4$ mV, $I_t = 50$ pA) (**e**). The FFT of the STM image of **e** is shown in the inset.

means of STS (observed here to be $2\Delta = 8$ meV centred at E_F). Superconductivity in $NbSe_2$, on the other hand, is significantly suppressed in the 2D limit, showing an onset of superconducting fluctuations at 1.9 K and a broadened superconducting transition with a midpoint at 0.65 K consistent with a Kosterlitz–Thouless transition. The one Nb antibonding band[6] that remains in the Fermi surface of single-layer $NbSe_2$ thus seems to play a critical role in the $NbSe_2$ CDW state, whereas the absent bands have a stronger influence on $NbSe_2$ superconductivity[17]. These results provide a window into the electronic structure of single-layer $NbSe_2$ and help to clarify the long-standing debate over $NbSe_2$ CDW formation.

Our experiments were carried out on high-quality submonolayer $NbSe_2$ films grown on epitaxial bilayer graphene (BLG) on 6H-SiC(0001), as sketched in Fig. 1a. The large-scale STM image in Fig. 1b shows the typical morphology of our single-layer $NbSe_2$ samples. Black regions correspond to the BLG substrate and the $NbSe_2$ layer is purple. The temperature dependence of the electronic ground state of single-layer $NbSe_2$ was measured by means of STM and electrical transport. Figure 1c–e shows STM topographic data for selected temperatures from $T = 45$ K to $T = 5$ K. At $T = 45$ K, well above the critical transition temperature for bulk $NbSe_2$ ($T_{CDW} = 33$ K), only the undistorted crystal structure is observed (Fig. 1c). At a lower temperature of $T = 25$ K, weak and spotty signatures of a superlattice are apparent (Fig. 1d). Here, small CDW patches surrounded by non-CDW regions can be seen. This is reminiscent of STM images of bulk $NbSe_2$ at temperatures close to the CDW transition temperature[19]. At $T = 5$ K, the 3×3 CDW superlattice is fully and uniformly developed for single-layer $NbSe_2$ (Fig. 1e). Figure 2 shows the temperature-dependent electrical resistance of single-layer $NbSe_2$ on BLG, acquired using a four-point probe low-excitation dc method (see Supplementary Information). No signature of the CDW transition is seen in the temperature dependence of the resistivity. Previous temperature-dependent resistivity measurements[19,29] for bulk $NbSe_2$ samples show a change in slope near the CDW onset temperature only for samples with large residual resistivity ratios. The absence of such a signature in the single-layer limit could be due to differences in the dominant electron scattering mechanism for bulk versus 2D samples. Importantly, a sharp downturn in the resistance begins at $T = 1.9$ K, indicative of the onset of superconducting fluctuations, the superconducting transition midpoint is at 0.65 K and the zero resistance point at 0.46 K, as shown inset. These data indicate that the trend of reduced superconducting transition temperature (T_c) with decreasing layer number in $NbSe_2$ (refs 11,12) continues down to the single-layer limit.

The alignment of the 3×3 CDW superlattice with the 1×1 atomic arrangement for single-layer $NbSe_2$ can be seen in Fig. 1e, similar to what has been seen previously in STM images of bulk $NbSe_2$ (refs 18,19,30). The 3×3 superlattice remains unchanged in our STM images, regardless of the orientation between the $NbSe_2$ layer and the BLG (see STM and LEED data in the Supplementary Information). This rules out the possibility that the 3×3 superlattice observed here in single-layer $NbSe_2$ is a moiré pattern (moiré patterns have been observed in $MoSe_2$/BLG (ref. 31)). A 3×3

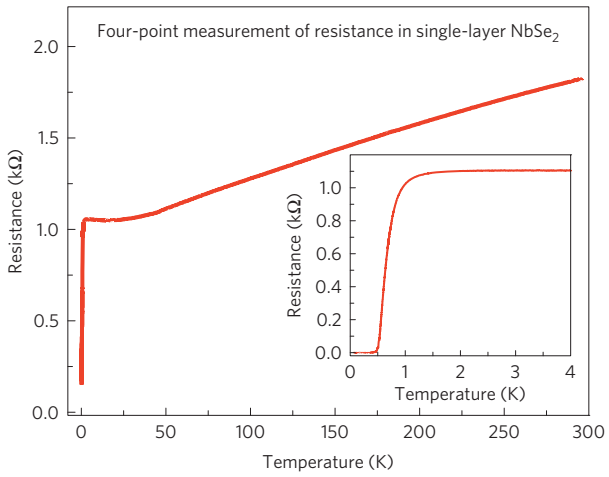

Figure 2 | Superconductivity in single-layer $NbSe_2$ on bilayer graphene. Four-point probe measurement of the temperature-dependent resistance of single-layer $NbSe_2$/BLG on insulating SiC(0001). Inset shows expanded view of R versus T between 0.05 and 4 K.

moiré pattern formation requires a quasi-commensurate match between overlayer and substrate atomic lattices, which does not occur here as $NbSe_2$ has a much larger unit cell than graphene. The rotational disorder we find in single-layer $NbSe_2$ with respect to the BLG substrate indicates weak coupling between them (similar weak coupling has been demonstrated for epitaxial graphene grown on different metal substrates[32]).

We experimentally determined the electronic structure of single-layer $NbSe_2$ by means of a combination of STS and ARPES. Figure 3a shows a typical STM dI/dV spectrum of single-layer $NbSe_2$ taken over a large bias range. In the positive bias (empty state) region the most pronounced feature is the peak labelled C_1 at $V_s = 0.5$ V. For negative bias (filled states) we observe a very shallow asymmetric peak near $V_s = -0.2$ V (labelled V_1), below which the local density of states (LDOS) flattens out and does not rise again until the peak labelled V_2 at $V_s = -0.8$ V. This behaviour is very different from previous STS results obtained for bulk $NbSe_2$, which show much higher LDOS in the region $-0.8\,\mathrm{V} < V < 0V$ (ref. 19). Figure 3b shows the ARPES data obtained from the same type of single-layer $NbSe_2$ sample as in Fig. 3a using *sp*-mixed polarized light. The measured electronic dispersion is energetically aligned with the dI/dV spectrum for comparison. Owing to rotational misalignment within

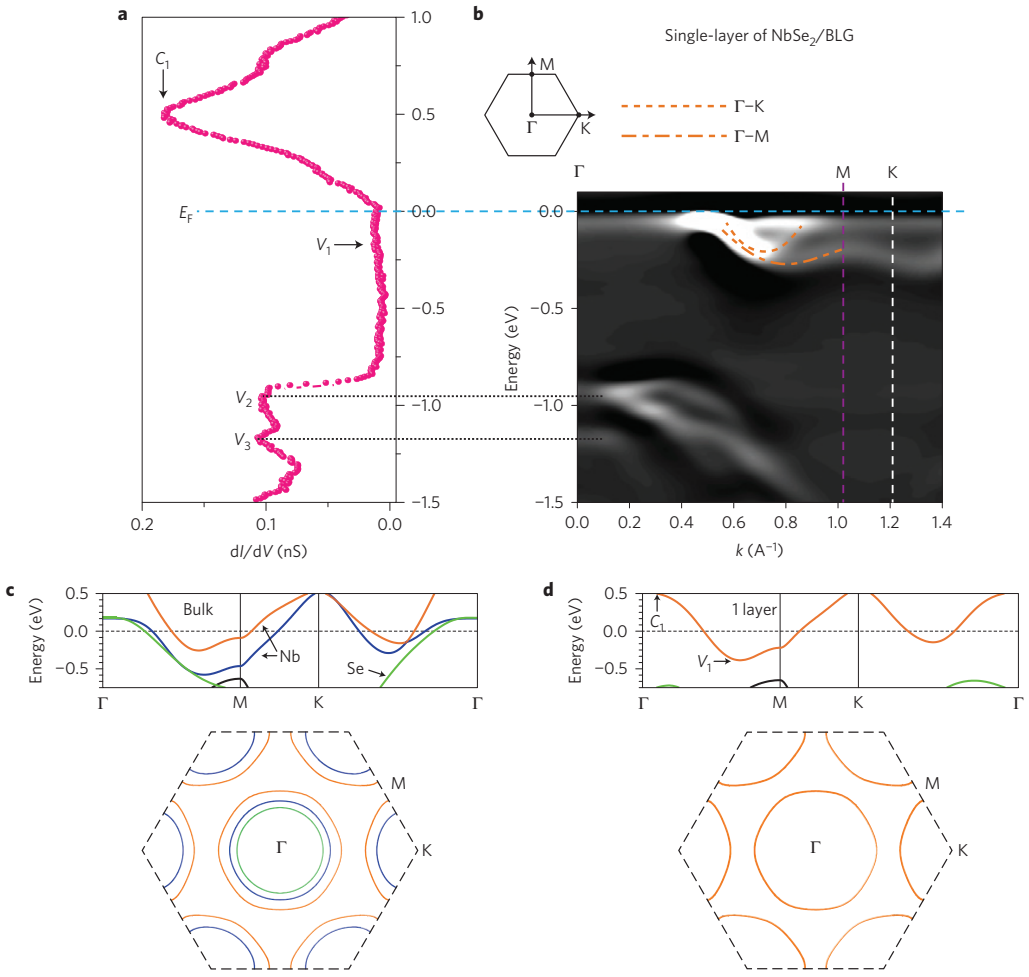

Figure 3 | Electronic structure of single-layer $NbSe_2$ on bilayer graphene. a, Wide-bias STM dI/dV spectrum acquired on single-layer $NbSe_2$/BLG showing several electronic features: V_{1-3} in the filled states and C_1 in the empty states ($f = 403$ Hz, $I_t = 100$ pA, $V_{r.m.s.} = 5$ mV, $T = 5$ K). **b**, Second-derivative *sp*-polarized ARPES dispersion of single-layer $NbSe_2$/BLG ($T = 300$ K) aligned in energy with the STM dI/dV curve shown in **a**. The dispersion exhibits angular integration due to the intrinsic rotational misalignment of $NbSe_2$ domains on the BLG substrate. The dotted and dot-dashed orange curves indicate bands from the Γ–K and Γ–M directions, respectively. The enhanced intensity near E_F is a well-known artefact of the second-derivative process and should not be confused with an electronic band. **c**,**d**, Predicted band structures and Fermi surfaces of bulk $NbSe_2$ (**c**) and single-layer $NbSe_2$ (**d**). The calculated band structures (DFT) have been adapted from ref. 6.

the $NbSe_2$ layer, the ARPES dispersion reflects a mixture of states with dominant intensity coming from the high-symmetry directions Γ–M and Γ–K. Two dispersive features can be seen crossing E_F (highlighted by the orange dashed lines). The ARPES spectrum also shows an energy gap over the range $-0.8\,eV < E < -0.3\,eV$, and below this several dispersive bands merge at the Γ point. In comparison, the ARPES spectrum for 5ML–$NbSe_2$ (see Supplementary Information) exhibits an additional Nb-derived band crossing the same energy range that is gapped for single-layer $NbSe_2$.

This experimental data is consistent with the changes in band structure that are predicted to occur when $NbSe_2$ is thinned down to a single layer[6]. The bulk $NbSe_2$ band structure (Fig. 3c) has three bands crossing E_F (two Nb-derived bands and one S-derived band), and exhibits no bandgap throughout our experimental energy range. Single-layer $NbSe_2$, on the other hand, has a much simpler predicted electronic structure (Fig. 3d), consisting of just one Nb-derived band crossing E_F away from the Γ point, as well as a bandgap from −0.4 to −0.8 eV and valence bands below that. These predicted features can be seen in our experimental ARPES dispersion (Fig. 3b) which shows that states right below E_F are located away from the Γ point, there exists an energy gap between −0.3 and −0.8 eV, and there exist several valence bands below −0.8 eV. Our dI/dV spectroscopy (Fig. 3a) is also consistent with the predicted single-layer band structure. For example, the peak at C_1 is consistent with the high DOS associated with the top of the Nb-derived band at Γ above E_F. We can also associate the shallow peak at V_1 with the Nb band right below E_F. The flat dI/dV region seen between V_1 and V_2 is consistent with the predicted bandgap (the fact that the dI/dV does not reach zero is due to residual tunnelling into the BLG substrate), and the peaks at V_2 and V_3 are consistent with the lower-energy valence band structure[6,33]. Overall, these features are very different from previous STS spectra obtained for bulk $NbSe_2$, which show much higher LDOS below E_F and no signs of a bandgap in the filled-state regions[19]. This is due to the additional electronic bands and resulting DOS expected in this energy range for bulk $NbSe_2$ as compared to single-layer $NbSe_2$ (Fig. 3c,d). This is also reflected in the additional band that can be seen in the ARPES spectrum of 5ML–$NbSe_2$ (Supplementary Information), which corresponds to a Nb bonding band (the blue band in Fig. 3c,d). The Se-derived band (green band in Fig. 3c,d) is typically not observed in ARPES owing to the high k_z dispersion.

To better understand the collective ground states of single-layer $NbSe_2$, we experimentally probed its low-energy electronic structure near E_F by means of STS. Figure 4 shows a typical low-bias dI/dV spectrum obtained for single-layer $NbSe_2$. This spectrum exhibits a striking energy gap feature centred at E_F that is not present in the calculated band structure of single-layer $NbSe_2$ (Fig. 3d). This feature, which is also not observed experimentally in bulk $NbSe_2$ (refs 18,27,28), exhibits a sharp dip at E_F bounded by two narrow peaks that sit on top of an asymmetric background. The dip at E_F does not reach all the way to zero, suggesting that it is not a full gap in the electronic structure. These STS features (including both wide-bias and low-bias spectra) were observed consistently for hundreds of dI/dV curves measured on several samples using a variety of different tip apexes. However, the width (2Δ) of the low-bias gap feature was found to exhibit some spatial variation, probably due to heterogeneity induced by the presence of defects at the $NbSe_2$/graphene interface (see Fig. 5c). Statistical analysis of data (257 curves) obtained at many different locations for $T = 5$ K yields an average gap value of $\Delta = 4.0$ mV with a standard deviation of 1 mV (the gap magnitude is defined as half the energy distance between the two peaks bracketing the gap). This value is in agreement with anisotropic gap-opening observed previously by low-temperature ARPES (ref. 17) at the Fermi surface near the K point in the band that is predicted to remain in the 2D single-layer limit of $NbSe_2$ (orange band in Fig. 3d).

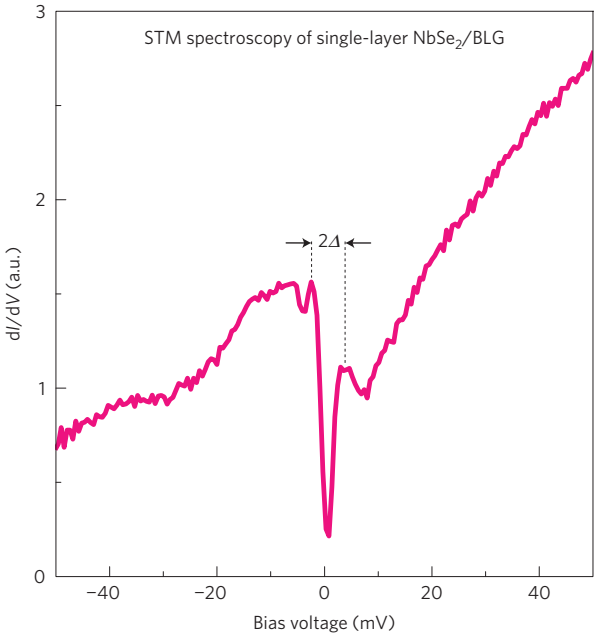

Figure 4 | CDW gap of single-layer $NbSe_2$. Low-bias STM dI/dV spectrum acquired on single-layer $NbSe_2$/BLG showing the CDW gap (Δ) at E_F ($f = 871$ Hz, $I_t = 100$ pA, $V_{r.m.s.} = 0.6$ mV, $T = 5$ K). The dashed lines indicate the positions of the CDW coherence peaks.

To better understand the origin of the E_F gap feature of Fig. 4, we performed spatially resolved dI/dV mapping of single-layer $NbSe_2$ at different bias voltages near E_F. Figure 5a,b shows dI/dV conductance maps of the same region taken at bias voltages outside ($V_b = -26$ mV) and inside ($V_b = 3$ mV) the low-bias gap region (Fig. 5c shows STM topography for this same region). The dI/dV conductance map taken at an energy outside of the gap (Fig. 5a) clearly shows the 3×3 CDW pattern, but the conductance map measured at an energy inside of the gap (Fig. 5b) shows no sign of the CDW. We Fourier analysed dI/dV maps taken at different voltages to obtain a more quantitative understanding of the energy dependence of CDW electronic features. Figure 5d shows the relative intensity of the resulting 3×3 peaks ($I_{3\times3}$) in the FFTs normalized to the intensity of the 1×1 Bragg peaks (I_{Bragg}). This ratio ($I_{3\times3}/I_{Bragg}(E)$) is a measure of the strength of the CDW modulation on the density of states and would remain constant if the gap had a different origin, such as electronic correlations. As seen in Fig. 5d, $I_{3\times3}/I_{Bragg}$ has large amplitude at energies far from E_F, but shows a decrease of nearly two orders of magnitude very close to E_F. Figure 5e shows a higher-resolution plot of the dip in $I_{3\times3}/I_{Bragg}$ at E_F (boxed region in Fig. 5d). The decrease in the ratio $I_{3\times3}/I_{Bragg}$ is seen to follow the energy dependence of the low-bias gap feature observed in dI/dV spectroscopy. This correlation of CDW intensity with gap energy dependence suggests that the gap is the result of CDW order. In particular, the diminishing CDW intensity for in-gap energies suggests that the residual LDOS within the gap arises from a portion of the Fermi surface that is not gapped by CDW order.

Our results allow us to draw some conclusions regarding different models of CDW formation in $NbSe_2$. First, we rule out recently proposed dimensionality effects on the CDW phase that were predicted for single-layer $NbSe_2$ but that are not observed here. This includes a predicted reduction of the CDW wavevector in the 2D limit[6]. We also rule out proposed Fermi-surface nesting mechanisms[19,21,22,24] involving the inner pockets around Γ and K (blue band in Fig. 3c) as these bands are not present in the single-layer limit and the CDW remains unchanged. As saddle-point-based mechanisms of CDW formation[23,26] involve the Fermi pockets that are still present in the

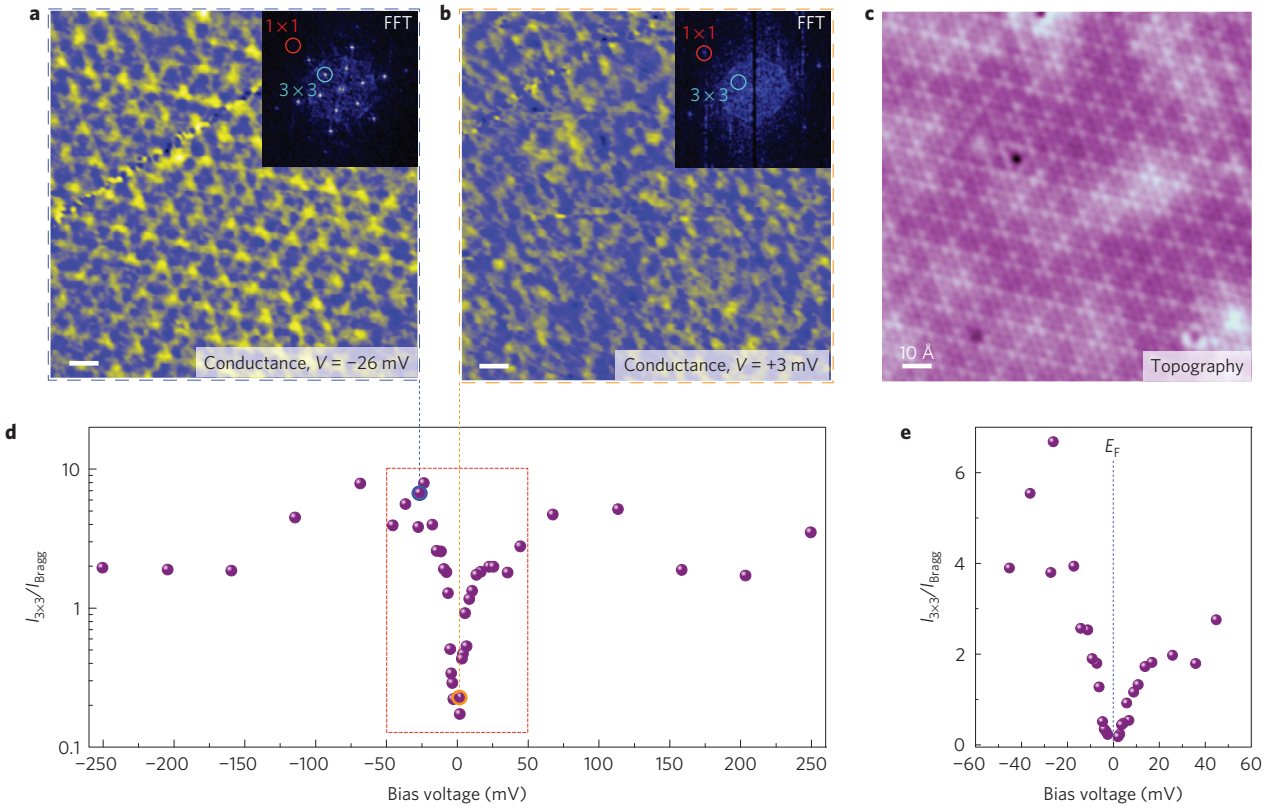

Figure 5 | Spatially and energetically resolved CDW phase in single-layer $NbSe_2$. a,**b**, Experimental conductance maps taken at $V_s = -26$ mV (**a**) and $V_s = +3$ mV (**b**) ($f = 871$ Hz, $I_t = 40$ pA, $V_{r.m.s.} = 0.6$ mV, $T = 5$ K). The FFT of each conductance map is shown as an inset, allowing identification of Bragg (1 × 1) and CDW (3 × 3) peaks. **c**, STM topograph of the same region where the conductance maps in **a** and **b** were acquired ($V_s = -17$ mV, $I_t = 40$ pA, $T = 5$ K). **d**, Logarithmic plot of the intensity of the 3 × 3 peaks ($I_{3\times3}$) in the FFT of the different conductance maps normalized by the Bragg peak intensity (I_{Bragg}) as a function of bias voltage. **e**, Linear scale zoom-in of the boxed region in **d**.

single-layer limit, we cannot rule them out based on fermiology. However, these mechanisms predict a CDW gap centred at an energy tens of meV away from E_F, and thus are inconsistent with our observation that the CDW gap is centred at E_F.

Our data also bring out some puzzling features concerning the CDW in $NbSe_2$. On the one hand, our observations that the gap is tethered to the Fermi energy, which is rather small, and that it correlates with the CDW amplitude are all consistent with the notion that the gap is the result of Fermi-surface nesting. On the other hand, our observation that the CDW modulation is observed in the LDOS at biases far exceeding the gap edges suggests that the CDW order is not a weak-coupling phenomenon arising from Fermi-surface nesting. This dual nature of the CDW gap imposes stringent constraints on any future theory of CDW formation in $NbSe_2$.

The suppression of the superconducting onset temperature in single-layer $NbSe_2$ is consistent with the trend previously observed[11–13], namely that the superconducting transition temperature decreases with sample thinning. Possible reasons for this include enhancement of thermally driven superconducting phase fluctuations, as well as weakening of the strength of Cooper pairing in two dimensions. Additional factors that may contribute to this weakening are the reduced screening of the Coulomb interaction[12] and the reduction of DOS at E_F for single-layer $NbSe_2$ arising from band reduction. It is likely that the electronic bands that are absent in single-layer $NbSe_2$ play a key role for thicker $NbSe_2$ films[17].

Methods

Methods and any associated references are available in the online version of the paper.

Received 27 June 2015; accepted 21 September 2015; published online 2 November 2015

References

1. Frohlich, H. Electrons in lattice fields. *Adv. Phys.* **3,** 325–361 (1954).
2. Peierls, R. E. *Quantum Theory of Solids* (Clarendon, 1955).
3. Guo, Y. *et al.* Superconductivity modulated by quantum size effects. *Science* **306,** 1915–1917 (2004).
4. Qin, S. Y., Kim, J., Niu, Q. & Shih, C. K. Superconductivity at the two-dimensional limit. *Science* **324,** 1314–1317 (2009).
5. Bose, S. *et al.* Observation of shell effects in superconducting nanoparticles of Sn. *Nature Mater.* **9,** 550–554 (2010).
6. Calandra, M., Mazin, I. I. & Mauri, F. Effect of dimensionality on the charge-density wave in few-layer 2H- $NbSe_2$. *Phys. Rev. B* **80,** 241108 (2009).
7. Lebegue, S. & Eriksson, O. Electronic structure of two-dimensional crystals from *ab initio* theory. *Phys. Rev. B* **79,** 115409 (2009).
8. Darancet, P., Millis, A. J. & Marianetti, C. A. Three-dimensional metallic and two-dimensional insulating behaviour in octahedral tantalum dichalcogenides. *Phys. Rev. B* **90,** 045134 (2014).
9. Peng, J. P. *et al.* Molecular beam epitaxy growth and scanning tunneling microscopy study of $TiSe_2$ ultrathin films. *Phys. Rev. B* **91,** 121113 (2015).
10. Novoselov, K. S. *et al.* Two-dimensional atomic crystals. *Proc. Natl Acad. Sci. USA* **102,** 10451–10453 (2005).
11. Frindt, R. F. Superconductivity in ultrathin $NbSe_2$ layers. *Phys. Rev. Lett.* **28,** 299–301 (1972).
12. Staley, N. E. *et al.* Electric field effect on superconductivity in atomically thin flakes of $NbSe_2$. *Phys. Rev. B* **80,** 184505 (2009).
13. Cao, Y. *et al.* Quality heterostructures from two dimensional crystals unstable in air by their assembly in inert atmosphere. *Nano Lett.* **15,** 4914–4921 (2015).
14. Varma, C. M. & Simons, A. L. Strong-coupling theory of charge-density-wave transitions. *Phys. Rev. Lett.* **51,** 138–141 (1983).
15. Valla, T. *et al.* Quasiparticle spectra, charge-density waves, superconductivity, and electron-phonon coupling in 2H-$NbSe_2$. *Phys. Rev. Lett.* **92,** 086401 (2004).

16. Weber, F. *et al.* Extended phonon collapse and the origin of the charge-density wave in 2H-$NbSe_2$. *Phys. Rev. Lett.* **107,** 107403 (2011).
17. Rahn, D. J. *et al.* Gaps and kinks in the electronic structure of the superconductor 2H- $NbSe_2$ from angle-resolved photoemission at 1 K. *Phys. Rev. B* **85,** 224532 (2012).
18. Soumyanarayanan, A. *et al.* Quantum phase transition from triangular to stripe charge order in $NbSe_2$. *Proc. Natl Acad. Sci. USA* **110,** 1623–1627 (2013).
19. Arguello, C. J. *et al.* Visualizing the charge density wave transition in 2H-$NbSe_2$ in real space. *Phys. Rev. B* **89,** 235115 (2014).
20. Arguello, C. J. *et al.* Quasiparticle interference, quasiparticle interactions, and the origin of the charge density wave in 2H- $NbSe_2$. *Phys. Rev. Lett.* **114,** 037001 (2015).
21. Wilson, J. A., Disalvo, F. J. & Mahajan, S. Charge-density waves in metallic, layered, transition-metal dichalcogenides. *Phys. Rev. Lett.* **32,** 882–885 (1974).
22. Straub, T. *et al.* Charge-density-wave mechanism in 2H-$NbSe_2$: Photoemission results. *Phys. Rev. Lett.* **82,** 4504–4507 (1999).
23. Shen, D. W. *et al.* Primary role of the barely occupied states in the charge density wave formation of $NbSe_2$. *Phys. Rev. Lett.* **101,** 226406 (2008).
24. Borisenko, S. V. *et al.* Two energy gaps and fermi-surface "Arcs" in $NbSe_2$. *Phys. Rev. Lett.* **102,** 166402 (2009).
25. Rice, T. M. & Scott, G. K. New mechanism for a charge-density-wave instability. *Phys. Rev. Lett.* **35,** 120–123 (1975).
26. Kiss, T. *et al.* Charge-order-maximized momentum-dependent superconductivity. *Nature Phys.* **3,** 720–725 (2007).
27. Chen, W. *et al.* Energy gaps measured by scanning tunneling microscopy. *Phys. Rev. B* **42,** 8890–8906 (1990).
28. Hess, H. F., Robinson, R. B. & Waszczak, J. V. STM spectroscopy of vortex cores and the flux lattice. *Physica B* **169,** 422–431 (1991).
29. Harper, J. M. E., Geballe, T. H. & Disalvo, F. J. Heat-capacity of 2H-N $NbSe_2$ at charge-density wave transition. *Phys. Lett. A* **54,** 27–28 (1975).
30. Giambattista, B. *et al.* Charge-density waves observed at 4.2 K by scanning-tunneling microscopy. *Phys. Rev. B* **37,** 2741–2744 (1988).
31. Ugeda, M. M. *et al.* Giant bandgap renormalization and excitonic effects in a monolayer transition metal dichalcogenide semiconductor. *Nature Mater.* **13,** 1091–1095 (2014).
32. Wintterlin, J. & Bocquet, M. L. Graphene on metal surfaces. *Surf. Sci.* **603,** 1841–1852 (2009).
33. Johannes, M. D., Mazin, I. I. & Howells, C. A. Fermi-surface nesting and the origin of the charge-density wave in $NbSe_2$. *Phys. Rev. B* **73,** 205102 (2006).

Acknowledgements

Research supported in part by the Director, Office of Energy Research, Materials Sciences and Engineering Division, of the US Department of Energy (DOE), under grant DE-AC02-05CH11231 supporting the sp2-bonded Materials Program (STM imaging and transport), and by the National Science Foundation under award # DMR-1206512 (STS spectroscopic analysis). Work at the ALS is supported by DOE BES under Contract No. DE-AC02-05CH11231. H.R. acknowledges support from Max Planck Korea/POSTECH Research Initiative of NRF, Korea. M.T.E. is supported by the ARC Laureate Fellowship project (FL120100038). A.R. acknowledges fellowship support by the Austrian Science Fund (FWF): J3026-N16.

Author contributions

M.M.U. and A.J.B. conceived the work and designed the research strategy. M.M.U., A.J.B., Y.C., W.R. and M.T.E. measured and analysed the STM/STS data. Y.Z., H.R. and S.-K.M. performed the MBE growth and ARPES and LEED characterization of the samples. S.O., C.O.-A., M.M.U. and Y.C. carried out the transport experiments. H.-Z.T. and A.R. helped in the experiments. D.L. participated in the interpretation of the experimental data. Z.H. and Z.-X.S. supervised the MBE and sample characterization. A.Z. supervised the transport measurements. M.F.C. supervised the STM/STS experiments. M.M.U. wrote the paper with help from M.F.C. and A.Z. M.M.U. and M.F.C. coordinated the collaboration. All authors contributed to the scientific discussion and manuscript revisions.

Additional information

Supplementary information is available in the online version of the paper. Reprints and permissions information is available online at www.nature.com/reprints. Correspondence and requests for materials should be addressed to M.M.U. or M.F.C.

Competing financial interests

The authors declare no competing financial interests.

Methods

Single-layer $NbSe_2$ was grown by molecular beam epitaxy (MBE) on epitaxial BLG on 6H-SiC(0001) at the HERS endstation of beamline 10.0.1, Advanced Light Source, Lawrence Berkeley National Laboratory (the MBE chamber had a base pressure of $\sim 2 \times 10^{-10}$ torr). We used SiC wafers with two different resistivities, $\rho \sim 300\ \Omega$ cm (STM and ARPES experiments) and $\rho > 10^8\ \Omega$ cm (transport and STM experiments). The morphology of the single-layer $NbSe_2$ was the same in both cases. The epitaxial BLG substrate was prepared by following the procedure detailed in refs 31,34. High-purity Nb and Se were evaporated from an electron-beam evaporator and a standard Knudsen cell, respectively. The flux ratio of Nb to Se was controlled to be ~1:30. The growth process was monitored by *in situ* RHEED and the growth rate was ~17 min per monolayer. During the growth the substrate temperature was kept at 600 K, and after growth the sample was annealed to 670 K. Low-energy electron diffraction (LEED) patterns were routinely taken after the growth to determine the quality of the sample (see Supplementary Information). Subsequent characterization by ARPES and core-level spectroscopy were performed in the analysis chamber (base pressure $\sim 3 \times 10^{-11}$ torr) of the 10.0.1 beamline. To protect the film from contamination and oxidation during transport through air to the ultrahigh vacuum scanning tunnelling microscopy (UHV-STM) chamber, a Se capping layer with a thickness of ~10 nm was deposited on the sample surface after growth. For subsequent STM and transport experiments the Se capping layer was removed by annealing the sample to ~600 K in the UHV STM system for 30 min. STM imaging and STS experiments were performed in an in-house-built UHV-STM operated at $T = 5$ K. STM differential conductance (dI/dV) spectra were measured at 5 K using standard lock-in techniques. To avoid tip artefacts, the STM tip was calibrated by measuring reference spectra on the graphene substrate[31]. STM/STS data were analysed and rendered using WSxM software[35].

Four-probe contacts for transport measurements were placed on the sample by electron-beam evaporation of 6.5 nm Ti and 100 nm Au through a shadow mask onto exposed graphene portions of the $NbSe_2$ sample (with a Se capping layer, see Supplementary Information). The Se capping layer was then removed in UHV and resistance measurements were subsequently performed either *in situ* inside the STM chamber, or in a Quantum Design PPMS dilution refrigerator (employing a rapid transfer from the UHV chamber to the inert gas/vacuum PPMS chamber). Measurements were made using a Keithley 2602A SourceMeter unit and a Keithley 181 nanovoltmeter with a current bias of 100 nA. At each temperature point the voltage was measured at both 100 nA and −100 nA to remove thermoelectric voltages induced by the temperature difference between the sample and measurement electronics. The heating rate during measurement ranged from 1 K h^{-1} to 60 K h^{-1}.

References

34. Wang, Q. Y. *et al.* Large-scale uniform bilayer graphene prepared by vacuum graphitization of 6H-SiC (0001) substrates. *J. Phys. Condens. Mater.* **25,** 095002 (2013).
35. Horcas, I. *et al.* WSXM: A software forscanning probe microscopy and a tool for nanotechnology. *Rev. Sci. Instrum.* **78,** 013705 (2007).